# Evolving the [Myoglobin, Cytochrome b_5] Complex from Dynamic toward Simple Docking: Charging the Electron Transfer Reactive Patch

Ethan N. Trana, Judith M. Nocek, Amanda K. Knutson, and Brian M. Hoffman*

Department of Chemistry, Northwestern University, Evanston, Illinois 60208, United States

S *Supporting Information*

ABSTRACT: We describe photoinitiated electron transfer (ET) from a suite of Zn-substituted myoglobin (Mb) variants to cytochrome b_5 (b_5). An electrostatic interface redesign strategy has led to the introduction of positive charges into the vicinity of the heme edge through D/E → K charge-reversal mutation combinations at "hot spot" residues (D44, D60, and E85), augmented by the elimination of negative charges from Mb or b_5 by neutralization of heme propionates. These variations create an unprecedentedly large range in the product of the ET partners' total charges ($-5 < -q_{Mb}q_{b_5} < 40$). The binding affinity (K_a) increases 1000-fold as $-q_{Mb}q_{b_5}$ increases through this range and exhibits a surprisingly simple, exponential dependence on $-q_{Mb}q_{b_5}$. This is explained in terms of electrostatic interactions between a "charged reactive patch" (crp) on each partner's surface, defined as a compact region around the heme edge that (i) contains the total protein charge of each variant and (ii) encompasses a major fraction of the "reactive region" (Rr) comprising surface atoms with large matrix elements for electron tunneling to the heme. As $-q_{Mb}q_{b_5}$ increases, the complex undergoes a transition from fast to slow-exchange dynamics on the triplet ET time scale, with a correlated progression in the rate constants for intracomplex (k_{et}) and bimolecular (k_2) ET. This progression is analyzed by integrating the crp and Rr descriptions of ET into the textbook steady-state treatment of reversible binding between partners that undergo intracomplex ET and found to encompass the full range of behaviors predicted by the model. The generality of this approach is demonstrated by its application to the extensive body of data for the ET complex between the photosynthetic reaction center and cytochrome c_2. Deviations from this model also are discussed.
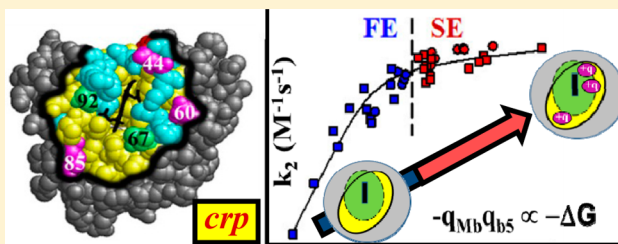
Protein–protein binding is at the heart of much of biology, with affinity constants ranging over many orders of magnitude[1,2] and many diseases involving the disruption and/or elimination of vital interactions.[3–6] Two limiting energy landscapes (Figure 1) have been used to describe the correlation between protein–protein binding and interprotein reactivity. (i) Weakly bound complexes can exhibit "dynamic docking" (DD), where reactive configurations are rare and geometrically distinct from more abundant, thermodynamically favored unreact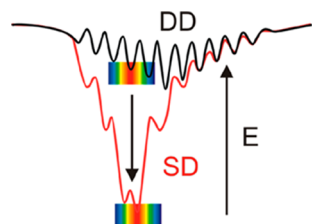ive configurations, and thus, binding and reactivity are decoupled.[7–10] (ii) Tightly bound complexes can exhibit "simple docking" (SD) in which a dominant, strongly binding configuration is also the most reactive.[7] We are exploring the principles governing reactive protein–protein binding by undertaking a systematic redesign of the interface of the [myoglobin (Mb), cytochrome b_5 (b_5)] electron transfer (ET) complex, with the aim of taking this weakly bound complex and strengthening the binding of reactive configurations, to evolve the DD landscape on which it functions into an SD landscape and thereby enhance ET.[11–13]

A reverse process, the identification of "hot spot" residues that provide the most favorable interactions in the protein–protein interface of a tightly bound, SD complex, is typically conducted through inspection of an X-ray structure, coupled with a traditional alanine replacement strategy.[14–17] The studies of Okamura and co-workers with the [photosynthetic reaction center (RC), cytochrome c_2 (c_2)] ET complex provide a compelling example of the use of this crystallographic/mutational strategy to study the coupling between binding

Figure 1. Energy landscapes for DD-type and SD-type reactions. The rainbow indicates ET reactive configurations, where red indicates the most ET-active geometries and wells represent stable ones.

affinity and ET. By employing both charged[18,19] and hydrophobic[20] interface mutants, they were able to identify residues essential to tight binding by monitoring mutationally induced changes in ET, with the elimination of hot spot interactions lowering the binding constant by more than 3 orders of magnitude relative to that of the wild-type complex. They further developed an empirical function to correlate the corresponding changes in binding affinity and ET reactivity generated by these interface mutations.[20]

Taking a weakly bound complex that reacts on a DD landscape and identifying potential hot spot surface residues where interactions can be most successfully introduced to evolve the complex toward a tight-binding complex with SD behavior presents a challenge of a different order. Weakly bound protein pairs such as the [Mb, b_5] ET complex ($K_a \sim 10^3$ M^{-1})[21,22] do not in general form crystals, precluding the use of X-ray structures to identify sites at which modification would stabilize the protein−protein interface and enhance reactivity. Indeed, such complexes do not even have a well-defined "structure".[23,24] This has led us to develop an interface redesign strategy that employs Brownian dynamics (BD) docking simulations to identify positions at which charge-reversal mutations will strengthen electrostatic interactions[25−27] in the protein−protein interface of ET-active conformations of such transiently formed, DD-type complexes.[13] Application of this strategy to the [Mb, b_5] partners identified residues D44, D60, and E85 of Mb as surface residue hot spots where the progressive introduction of D/E → K mutations in the vicinity of the Mb heme edge should create a positively charged "patch"[28] on the Mb surface with enhanced Coulombic attraction to the complementary pattern of negative surface charges on the b_5 template, progressively stabilizing reactive configurations of the complex and "evolving" it toward a reactive SD behavior (Figure 1).

Guided by these predictions, we have now prepared all seven mutants in which positive charges have been added to the Mb surface by D/E → K charge-reversal mutations at one, two, or all three of the hot spot positions on Mb, augmented with variants in which negative charge is eliminated from the Mb surface by neutralization of the Mb heme propionates. The binding affinity and ET reactivity for each member of this suite have been measured at two different pH values by examination of ET quenching of the Zn-deuteroporphyrin IX (ZnD) or ZnD-(dimethyl ester)-reconstituted Mb photodonors by either the ferri-b_5 electron acceptor or its diester heme-reconstituted analogue.

Whereas b_5(wt) has a large negative total charge ($q_{b_5}e = -5.7$ e), Mb(wt) is nearly charge neutral ($q_{Mb}e = -0.3$ e) [pH 7 (Table SI_1 of the Supporting Information)]. The charge variation through mutation and/or heme neutralization yields a set of [Mb, b_5] complexes that spans an unprecedentedly large range in the product of the total charges on the partners ($-5 < -q_{Mb}q_{b_5} < 40$) (Table SI_1 of the Supporting Information). As $-q_{Mb}q_{b_5}$ increases within the set, the binding constant (K_a) increases by more than 3 orders of magnitude and the complexes shift from the fast-exchange (FE) dynamics regime to the slow-exchange (SE) regime on the triplet-state ET time scale. The second-order ET rate constant (k_2) concomitantly increases by ∼10^3; intracomplex protein−protein ET is observed in the SE regime, and it too increases with $-q_{Mb}q_{b_5}$. The correlated increases in binding and reactivity are found to have remarkably simple dependencies on the charge product,

$-q_{Mb}q_{b_5}$. To describe these consequences of charge buildup, we have been led to extend the idea of a charged patch[28−31] by defining a charged reactive patch (crp) on each protein that satisfies two criteria. (i) It is the most compact area that surrounds a selected surface point/region and in which the surface charge of the protein equals its total charge. (ii) The selected region, here taken to be the heme edge, is chosen so that the crp encompasses a major fraction of the ET-active surface, the "reactive region (Rr)" comprising the surface atoms with large matrix elements for electron tunneling to the heme (Figure 2). Because the hot spot mutation sites of Mb and the
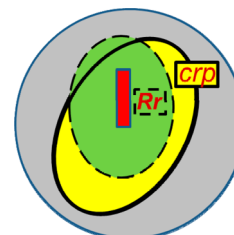

Figure 2. Cartoon of the overlapping charge reactive patch (crp) and reactive region (Rr).

heme propionates of both partners fall within their WT crp, the crp for each of the ET partners remains compact and essentially invariant as its surface charge is changed. With the crp of each partner of every complex containing its total protein charge, while the remaining surface has no net charge, complex formation can be treated in terms of the interaction between the total charges, localized within the complementary, reactive regions on the protein surface, the crp. The correlated progression of k_2 and K_a with increasing $-q_{Mb}q_{b_5}$ and the transition from fast- to slow-exchange dynamics then arise naturally when the crp description of protein−protein binding is integrated into the textbook steady-state treatment of reversible pre-equilibrium binding between partners that exhibit intracomplex ET.[32−34]

This simple approach completely captures the global aspects of the correlated electrostatic control of binding and reactivity, while at the same time illuminating the "granularity" that results from alternative arrangements of charges on the Mb surface. The generality of this approach is evidenced by its ability to treat the correlated decreases in binding and ET rate constants between the reaction center (RC) and cytochrome c_2 (c_2), as produced by separate suites of hydrophobic and electrostatic mutations within the interface.

■ MATERIALS AND METHODS

Bacterial Strains and Plasmids. *Escherichia coli* strains DH5a and BL21(DE3) were used for plasmid propagation and protein expression, respectively. Coding sequences for target proteins were cloned under control of the T7*lac* promoter by placing the initiation codon at the *Nco*I site of pET28a$^{(+)}$ (Novagen), which confers resistance to kanamycin. The plasmid for expressing horse heart myoglobin (Mb) was obtained from A. Grant Mauk (University of British Columbia, Vancouver, BC). The wild-type gene was then amplified via polymerase chain reaction (PCR) from constitutive expression vector pEMBL18 containing the template[35] with the forward (ACTAGCCATGGGTCTGTCTGATGGTGA) and reverse (ACTAGGGATCCTTAACCCTGGAAACCCAGTTC) pri-

mers. The PCR product was digested with *NcoI* and *BamHI* enzymes and cloned into the pET28a$^{(+)}$ vector, similarly digested with the same enzymes. Protein mutants were created via site-directed mutagenesis using a Stratagene QuikChange II XL Site-Directed Mutagenesis Kit. The constructs for wild-type Mb and all mutants were verified by DNA sequencing (SeqWright).

Expression and Purification. Terrific broth medium (0.17 mM KH$_2$PO$_4$, 0.72 mM K$_2$HPO$_4$, 12 g of tryptone, and 24 g of yeast extract/L) containing kanamycin (100 μg/mL) was inoculated with an overnight culture of BL21(DE3) *E. coli* transformed with the desired Mb construct. The culture was grown at 37 °C and 350 rpm until the OD$_{600}$ reached ~2.4–2.7. Protein expression was induced with IPTG (final concentration of 1 mM) and an increase in temperature to 42 °C. The resulting protein formed inclusion bodies as described by Ribeiro et al.[36] High cell densities (OD$_{600}$ > 6) are desired; to provide sufficient aeration of the expression culture, the volume of the culture was limited to <25% of the flask volume and a high shaking speed (>350 rpm) was maintained.

After 3 h, the culture was pelleted by centrifugation at 20000g for 15 min, resuspended (20 mL/L) in 100 mM Tris-HCl, 5 mM EDTA, and 1% Triton X-100 (pH 8.0), and lysed by sonication. This process was repeated three times with the same buffer, taking care to completely resuspend the pellet after each centrifugation step. The pellet was then resuspended in water and sonicated twice, as before, to remove excess Triton X-100. Finally, the pellet was resuspended in 100 mM Tris-HCl and 8 M guanidine chloride (pH 8.0) and sonicated to homogeneity.

An excess of the desired metalloporphyrin (Frontier Scientific) was added along with 5 mM sodium dithionite, and then very slowly as the mixture was being stirred, the volume was doubled with 100 mM Tris-HCl (pH 8.0). This solution was then dialyzed overnight in 14 L of 10 mM Tris-HCl (pH 7.2) with stirring. The next day, precipitated protein was removed by centrifugation, and the reconstituted Mb was further purified by ion-exchange chromatography, using a CM-52 column equilibrated with 10 mM Tris-HCl (pH 7.2). Purity was assayed by measuring the $A_{414,408}/A_{280}$ ratio and verified by sodium dodecyl sulfate–polyacrylamide gel electrophoresis. The protein was then exchanged into 10 mM KP$_i$ (pH 7.0), concentrated, pelleted in liquid nitrogen, and stored at −80 °C. The protein yield was found to be mutation-dependent and decreased with added mutations; the wild type was obtained at ~100 mg/L and the D44K/D60K/E85K mutant at ~50 mg/L. Concentrations were calculated using the Soret absorbance (ZnDMb, ZnDdmeMb, ε_{414} = 361 M^{-1} cm^{-1};[7] Fe^{3+}Mb, ε_{408} = 188 M^{-1} cm^{-1}).[37]

Bovine Fe$^{3+}b_5$ was expressed in *E. coli*, isolated, and purified according to previously described methods.[38,39]

Brownian Dynamics Simulations. Mutants were designed as described previously using a Brownian dynamics docking protocol implemented in the Linux version of MacroDox.[13] Total charges were calculated for each of the Mb and b_5 variants using the Tanford–Kirkwood method[40] with the default intrinsic pK_a values, adjusted as implemented in MacroDox[41] using the experimental parameters: (i) pH 7, μ = 18 mM, and 293 K and (ii) pH 6, μ = 5 mM, and 293 K. All Arg, Tyr, and Lys residues (including the mutation sites) were fully charged; all Asp and Glu residues were essentially deprotonated with the charge distributed between their carboxylate oxygen atoms. Consistent with the His pK_a values

measured by NMR for met-Mb(horse),[42,43] the computed pK_a for His 36 is larger than the default intrinsic pK_a of 6.3, while those for His 48 are lower than the intrinsic pK_a. The computed pK_a and corresponding charges on the N$_\varepsilon$ and N$_\delta$ atoms of the His residues are slightly smaller for the more highly charged mutants in comparison to their values in Mb(wt). The formal charges on the metal atoms in Mb and b_5 were assigned as +2 and +3, respectively. We have suggested previously that the pK_a of charged residues within the protein–protein interface may change upon binding,[7] but given the diversity of the geometries resulting from the BD simulations, this complication has not been addressed here.

Flash Photolysis Experiments. Cuvettes filled with 2 mL of buffer were stored open to the atmosphere overnight in a N$_2$-filled glovebox. Stock solutions of protein were thawed on a cold block in the glovebox for several hours prior to the experiment. The final concentration of Mb in the sample was 5 μM. Protein stock concentrations were determined using a Hewlett-Packard UV–vis spectrophotometer: ε_{414} (ZnDMb) = 361 mM^{-1} cm^{-1};[7] ε_{414} (Fe$^{3+}b_5$) = 117 mM^{-1} cm^{-1}.[44]

Samples were excited with a Nd:YAG Quanta-Ray INDI laser (Spectra-Physics) tuned to 532 nm. The output power was set so that it was approximately 100 mJ at the sample holder. Triplet quenching measurements were performed with an LKS.60 laser flash photolysis spectrometer (Applied Photophysics) fitted with a xenon lamp with pulsing capabilities. For slow triplet decays (<1000 s^{-1}), a setup modified from Applied Photophysics' stopped-flow instrument was employed with a nine-stage photomultiplier tube for detection. Data for shorter time scales were taken with an Agilent Infiniium 600 MHz digitizer and a five-stage photomultiplier tube detector. The xenon lamp was pulsed to achieve the shortest time scales. The triplet decay time courses were monitored at 475 nm. Typically, 10 shots were averaged on the slow time scale setup, and at least 20 shots were averaged for the fast setup data collection. All kinetic experiments were performed at 20 °C.

■ RESULTS AND DISCUSSION

Electron Transfer Measurements. In the absence of b_5, the photoexcited triplet states of all the ZnMbs decay exponentially, with a rate constant (k_d) that ranges from 50 to 500 s^{-1}. Upon addition of b_5, photoinitiated ET quenches the triplet excited state, with the form of the resulting triplet decay trace being dependent on the strength of the binding interaction. The traces are exponential throughout a quenching titration when binding is weak and the complex is in fast exchange (FE) with its components; they are biexponential when the binding has been strengthened to the point that the complex is in slow exchange (SE) with unbound partners. The top panel of Figure 3 shows triplet decay traces for a set of Mb surface charge mutants in solutions with excess b_5 ([b_5]/[Mb] = 2). The [Mb, b_5] pairs with low values of the protein–protein charge product ($-q_{Mb}q_{b_5} \leq 16.5$), e.g., [ZnMb(wt), b_5] and [ZnMb(D44K), b_5] (Table SI_1 of the Supporting Information), are all in the FE limit, and their triplet decay traces are described well by an exponential function. For these [Mb, b_5] pairs, the quenching rate constant (k_q) obtained by subtracting k_d from the observed rate constant (k_{obs}) increases linearly (Figure 3, bottom) as a function of [Fe$^{3+}b_5$]. The slope of the resultant line gives the bimolecular quenching rate constant, k_2. Complexes with high values of the charge product ($-q_{Mb}q_b > 16.5$), e.g., [ZnMb(44/60), b_5] and [ZnMb(44/60/85), b_5], fall
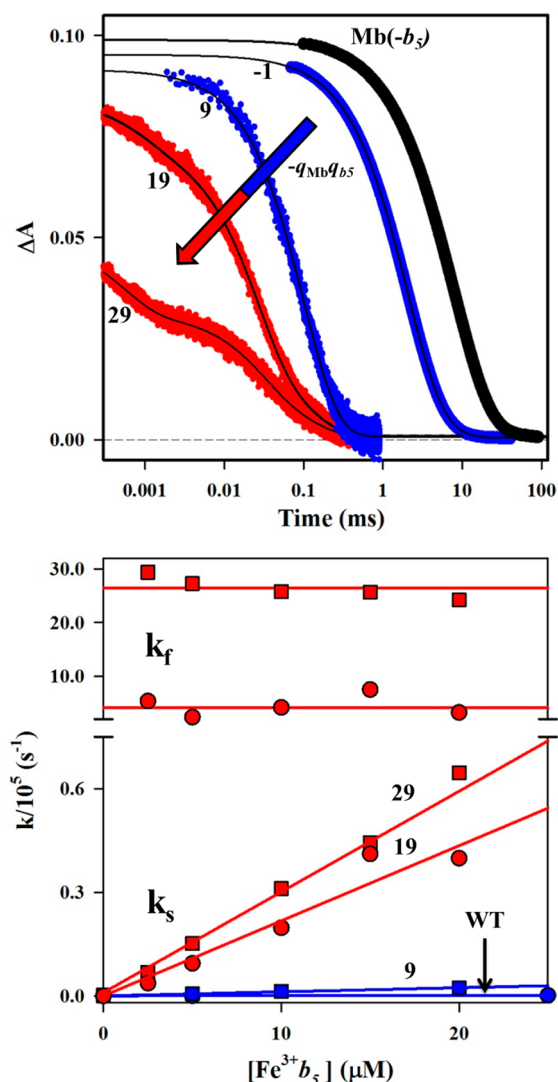
Figure 3. Triplet decay traces at $[b_5]/[Mb] = 2$ (top) and fit parameters during titrations of Mb with b_5 (bottom). Data for the Mb(wt) (circles) and Mb(+2) (squares) complexes, classified as FE (blue), were analyzed with a single-exponential decay function; the Mb(+4) (circles) and Mb(+6) (squares) complexes, classified as SE (red), were analyzed with a biexponential decay function. Conditions: 5 μM Mb, 5 mM KP$_i$, pH 6, 20 °C, and 475 nm.

in the SE regime, with biphasic triplet decay traces. For these complexes, the rate constant for the faster decay phase (k_f) is invariant with b_5 concentration (Figure 3, bottom) and is attributed to protein–protein ET within the preformed complex; the rate constant for the slower component (k_s) varies linearly with $[Fe^{3+}b_5]$, and like the single kinetic phase exhibited by the FE (DD)-type pairs, its slope (k_2) is associated with second-order ET quenching of the free ZnMb by $Fe^{3+}b_5$.

For the SE complexes, the fraction of the faster phase in the triplet decay typically is taken to correspond to the fraction of bound complex, and the measured variation in this fraction during a titration with an ET quencher is fit to a binding isotherm to determine the protein–protein binding constant, K_a. In contrast, K_a generally cannot be measured from a triplet quenching titration for complexes in the FE regime. However, we have shown that the progressive decrease in the early time absorbance (A_0) during a triplet-quenching titration results from quenching of the singlet state by b_5.[13] On the singlet time

scale, all the [Mb, b_5] complexes are in SE, and as a result, the variation in the absorbance decrease can be fit to a binding isotherm to calculate K_a, regardless of whether the complex is in FE or SE on the triplet time scale. This procedure has been applied to each of the complexes studied here.

The top panel of Figure 4 is a semilogarithmic plot of K_a for all the [Mb, b_5] complexes, measured at both pH 6 and 7, as a
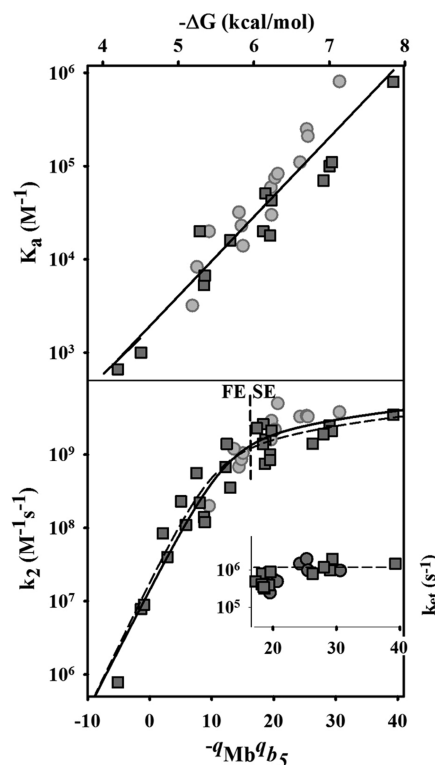

Figure 4. Dependence of K_a (top), k_2 (bottom), and k_{et} (inset in bottom panel) on the negative charge product ($-q_{Mb}q_{b_5}$) and corresponding driving force for binding, $-\Delta G$. The dashed line (bottom) indicates the experimentally observed division between the FE and SE regimes. Conditions: 5 mM KP$_i$ at pH 6 (light gray circles) or 10 mM KP$_i$ at pH 7 (dark gray squares). The solid line running through points of the bottom panel is a fit of the entire k_2 data set to eq 7; the dashed line is a fit to pH 7 data. The bimolecular quenching rate constants, ET rate constants, binding affinities, and charge products for all the [Mb, b_5] pairs included in this figure are listed in Table SI_1 of the Supporting Information. The fit parameters for the entire k_2 data set are discussed in the text.

function of the product of the total protein charges determined from Poisson–Boltzmann electrostatic computations, $-q_{Mb}q_{b_5}$. As $-q_{Mb}q_{b_5}$ increases from -5 to 40, the [Mb, b_5] complex binding affinity increases by nearly 3 orders of magnitude. The exponential increase in K_a revealed in this plot shows that the driving force for complex formation ($-\Delta G°_a = RT \ln K_a$) increases linearly with the total charge product for the [Mb, b_5] ET pairs, $-q_{Mb}q_{b_5}$. This surprisingly simple dependence on total protein charges confirms that the progressive increase in K_a is electrostatically driven and that the mutations change only the electrostatic interactions between the partners.

The bottom panel of Figure 4 is a semilogarithmic plot of k_2 versus $-q_{Mb}q_{b_5}$ for all complexes at both pH 6 and 7. At low values of $-q_{Mb}q_{b_5}$, where FE dynamics are obtained, k_2 varies

exponentially with $-q_{Mb}q_{b_5}$, increasing by more than 3 orders of magnitude, from 8.0×10^5 M^{-1} s^{-1} at $-q_{Mb}q_{b_5} = -5$ to 1.2×10^9 M^{-1} s^{-1} at $-q_{Mb}q_{b_5} \sim 16$. This behavior was observed previously for Mb mutants with $-q_{Mb}q_{b_5} \leq 12$.[7,45] As the charge product is increased beyond this value, the [Mb, b_5] pairs show SE-type dynamic behavior (Figure 3) and the increase in k_2 with $-q_{Mb}q_{b_5}$ slows markedly, resembling the weak charge dependence expected for the diffusion rate describing the association of charged partners.[32,46,47] The inset of the bottom panel of Figure 4 displays the intracomplex ET rate constant, k_{et}, measured for the complexes in the SE regime as a function of the charge product. Although $k_{et} \sim 10^6$ over the accessible range of $-q_{Mb}q_{b_5}$, closer examination reveals that k_{et} increases by nearly 1 order of magnitude in this range, from $\sim 2 \times 10^5$ s^{-1} to a limiting rate constant in excess of 10^6 s^{-1}.

Although k_2 increases smoothly with an increasing $-q_{Mb}q_{b_5}$, the dynamics of complex formation changes from FE to SE; complexes for which $-q_{Mb}q_{b_5} \leq 16.5$ show FE dynamics, and complexes with a larger value show SE dynamics. An interesting aspect of the presentation in Figure 4 is that an apparent pH dependence of k_2 for the [Mb, b_5] pairs (Table SI_1 of the Supporting Information) is shown to be merely a consequence of the differing pH dependencies of $-q_{Mb}q_{b_5}$ for each pair: the points for both pH values can be plotted together. Likewise, no special influences of heme neutralizations are seen beyond the resulting changes in $-q_{Mb}q_{b_5}$.

Analysis. The interface redesign strategy employed here leads to the progressive generation of a patch in the vicinity of the ET-active Mb heme edge with a high local density of positive charge, complementary to the high negative charge of the b_5 surface. Figure 4 shows that the consequence of this charge buildup is that K_a and k_2 for the suite of [Mb, b_5] complexes can be treated as functions of a single variable, the product of the total charges on the two partners, $-q_{Mb}q_{b_5}$. Although this confirms that binding and reactivity are both under electrostatic control, at first glance the simple logarithmic dependence of K_a on $-q_{Mb}q_{b_5}$, corresponding to a simple Coulombic interaction between total protein charges, is a surprise. One might expect that at relatively low values of $-q_{Mb}q_{b_5}$, where there has been little localized charge buildup, the electrostatic interactions would involve charges over a wide area, and not be so simply parametrizable.[48−50]

The development of a model for the observed behavior begins with the recognition that for all complexes studied, the measurements of both binding affinity and ET probe only configurations of the complex in which b_5 is bound at a site on the Mb surface that has a good ET pathway to the heme;[51] such sites comprise a reactive region (Rr) on the Mb surface surrounding its exposed heme edge. Considering first the binding constant, K_a, this restriction arises because binding is assayed by measuring singlet ET quenching. As this quenching process must compete with the intersystem crossing rate ($k_{isc} \sim 2 \times 10^8$ s^{-1}), it can report only on complexes with reactive configurations whose pathways for intracomplex ET can compete effectively, namely configurations in which b_5 is bound at the Rr. Figure 5A shows a Pathways coupling map for the Mb surface,[52] color-coded according to the magnitude of the matrix element for electron tunneling from that site to the heme iron. The heme edge, of course, has the largest tunneling
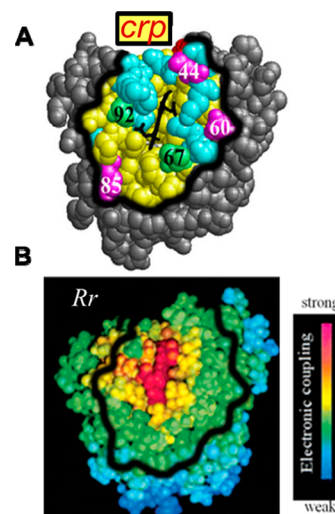

Figure 5. Mb charged reactive patch (crp) and Pathways coupling map. (A) Mb crp defined to include residues such that $q_{patch} \sim q_{Mb}$. This area includes all the surface residues within 10 Å of the heme. Color scheme: yellow for patch residues, red for acidic and blue for basic residues within the patch, gray for residues outside of the patch, magenta for charged hot spot mutation sites, and green for uncharged mutation sites. (B) Pathways coupling map and color scheme from Liang et al.[7] The thick black line shows the rough outline of the crp in panel A.

matrix element, with concentric "rings" of decreasing coupling as the distance from the heme increases. A more precise definition of the Rr could be developed, but for our purposes, one may loosely imagine that the Rr for Mb comprises the surface atoms colored red and yellow (or yellowish green) in Figure 5A.

A quantitative description of binding in terms of total protein charges is obtained by linking the idea of a Rr around the heme edge to total protein charge, through the definition of a charged reactive patch (crp). Although one might have expected that a wide area of the Mb surface contributes to the energetics of binding at low to moderate values of $-q_{Mb}q_{b_5}$, we have examined the surface of Mb and found that a compact surface region that surrounds its heme edge contains a net surface charge equal to the total charge of the wild-type protein, leaving the rest of the protein as charge-neutral. The well-defined surface region identified in this way, shown in both panels of Figure 5, includes the Mb surface atoms that are within ~ 10 Å of any heme atom. It encompasses (i) much of the Rr (Figure 5A), and thus an area whose effective ET pathways from the Mb surface support rapid electron tunneling between the heme of a bound b_5 and the Mb heme, and (ii) all of the Mb mutation sites employed in this study (Figure 5B). Thus, the total charge on every Mb charge variant can be treated as being concentrated within the crp. The corresponding crp for b_5 and its heme-neutralized charge variant, likewise defined to contain the total protein charge, is displayed in Figure SI_1 of the Supporting Information. The definition of a crp naturally leads to a picture in which the ET partners react only when the Rr's within their complementary crp's are electrostatically drawn together.

This picture is supported by the finding that the crp's of the two partners are relatively small and have effectively the same solvent-accessible surface area: 1410 Å^2 for Mb and 1560 Å^2 for b_5 at pH7. The crp on Mb includes only $\sim 22\%$ of the solvent-

accessible Mb surface, which supports the physical reality behind the concept of a well-defined patch at which both binding and reactivity occur. Furthermore, BD simulations show that as the charge product is increased, there is a corresponding large increase in the likelihood that a reactive configuration (BD "hit") involves binding through a protein–protein interface that includes the complementary crp of Mb and b_5 (Figure SI_2 of the Supporting Information). We, of course, recognize that one could use any surface location to define a charged patch that encompasses the total protein charge. What makes the crp construct useful is that reactivity is associated only with the Rr, which mostly is contained within the crp (Figures 2 and 5).

A simple formulation of the reactive, electrostatic binding between the crp of the partner proteins follows naturally. As ET quenching arises from binding of b_5 at surface sites of the Mb Rr that lie within its crp, and as the total charges for the Mb and b_5 partners are defined to be localized within the relatively small surface areas of their crp, the electrostatic driving force for reactive complex formation must be dominated by the Coulombic interaction between the charges within the complementary crp of the partner proteins. The further simplification of expressing this driving force as the electrostatic interaction of the total protein charges leads to a form for the driving force that corresponds to the experimental findings:

$$
\begin{aligned}
-\Delta G^\circ_a &= RT \ln(K_a) \\
&= -[\Delta G^\circ_{hyd} + V(q_{Mb}q_{b_5})] \\
&= -[\Delta G^\circ_{hyd} + q_{Mb}q_{b_5}f(\varepsilon_o, \varepsilon_i, r_{i,j})] \\
&= RT \ln K_0 - q_{Mb}q_{b_5}f(\varepsilon_o, \varepsilon_i, r_{i,j})
\end{aligned} \tag{1}
$$

Here we have taken the electrostatic interaction energy, $V(q_{Mb}q_{b_5})$, to be proportional to the product of the complementary patch charges ($q_{Mb}q_{b_5}$), and a function f that could be formulated at differing levels of sophistication in terms of the distances between charged Mb and b_5 patch residues ($r_{i,j}$) and the protein and solvent dielectrics (ε_o and ε_i, respectively), but whose modeling is far beyond the scope of this report.[53] The additional contribution, ΔG°_{hyd}, takes into account nonelectrostatic interactions, as well as an entropy term that reflects the low fractional surface area at which reaction can occur. Definition of such a term represents an extension of the partitioning of the binding free energy, discussed previously.[9] With this definition, the last line of eq 1 rewrites $-\Delta G^\circ_a$ in terms of K_0, the binding constant that would apply when Mb is completely uncharged ($q_{Mb} = 0$).

Equation 1 has been used to fit the dependence of K_a on $-q_{Mb}q_{b_5}$ for experiments at both pH 6 and 7. This fit yields a K_0 of 2×10^3 ($-\Delta G^\circ_a = 4.6$ kcal/mol) and an f of 0.093 kcal/mol; as shown in the top panel of Figure 4, it gives an excellent description of the ~1000-fold increase in K_a with an increasing $-q_{Mb}q_{b_5}$ over the entire range explored. Conversely, the experimentally observed linear dependence of $-\Delta G^\circ_a$ on $-q_{Mb}q_{b_5}$ supports the simplified description of electrostatic binding as governed by the total protein charge concentrated within the protein–protein interface formed by the complementary crp. We note, however, that because the actual magnitude of the parameter f is dependent on the spread in $-q_{Mb}q_{b_5}$, it might vary somewhat with the method for computing protein charges.[54] The success of this description (eq 1) further supports the implicit assumption that hydrophobic interactions between the partners remain largely invariant as the charge in the Mb crp is increased.

We next consider k_2, the bimolecular rate constant for ET. In the FE/DD regime, as we previously discussed,[7] k_2 can be written as the sum of rate constants for all individual configurations weighted by their individual binding constants (eq 2). Here, the nonreactive (NR) configurations are in the majority (N_{NR} in number), but they do not contribute to reactivity as $k_{NR} \sim 0$. Instead, the minority of reactive (R) conformations (n_R in number; large intracomplex ET rate constant, k_R) dominates the reactivity, leading to eq 3

$$
k_2 = \sum K_i k_i \sim n_R k_R K_R + N_{NR} k_{NR} K_{NR} \tag{2}
$$

$$
\sim n_R k_R K_R \tag{3}
$$

As the binding constant measured by ET quenching, K_a, monitors only reactive sites, one may equate K_a to K_R. Taken together, eqs 1 and 3 then predict the exponential dependence of k_2 on $-q_{Mb}q_{b_5}$ in the DD/FE regime that is observed (Figure 4). For the more tightly bound complexes that populate the SE regime, the interface redesign has enhanced binding to the ET-active R configurations sufficiently so that one directly observes the first-order, intracomplex ET rate constant (Figure 4, inset). As this monitors only configurations in which b_5 is bound to reactive sites within the crp, one can assign $k_{et} = k_R = k_f$, which is taken to be invariant with $-q_{Mb}q_{b_5}$.

The second-order rate constant (Figure 4, bottom), however, continues to increase with an increasing $-q_{Mb}q_{b_5}$ through the FE/SE transition and into the SE regime, but the rate of increase slows markedly. Understanding the full $-q_{Mb}q_{b_5}$ dependence of k_2, and in particular the transition from FE to SE, requires that the description of the dependence of the electrostatic binding energetics on $-q_{Mb}q_{b_5}$ be incorporated into a kinetic scheme. We find that this can be successfully conducted through the use of the textbook steady-state treatment of intracomplex ET between partners involved in a binding pre-equilibrium.

$$
D + A \underset{k_{off}}{\overset{k_{on}}{\rightleftharpoons}} DA \overset{k_{et}}{\rightarrow} D^+A^- \tag{4}
$$

This scheme predicts that in the limit of tight binding, intracomplex, photoinitiated ET will be first-order and its rate constant, k_{et}, will equal k_R. Most importantly, we find that it provides an excellent description of the variation of k_2 with $-q_{Mb}q_{b_5}$ over the full range of behaviors from FE and weak binding through the transition to SE and tight binding (Figure 4, top). The scheme of eq 4 leads to the classical steady-state expression for k_2 as a function of the intracomplex ET rate constant (k_{et}), the diffusion-limited association rate constant (k_{on}), and the affinity constant ($K_a = k_{on}/k_{off}$).

$$
\begin{aligned}
k_2 &= k_{et}k_{on}/(k_{et} + k_{off}) \\
&= k_{et}k_{on}K_a/(k_{on} + k_{et}K_a)
\end{aligned} \tag{5}
$$

In the FE limit, defined by the rate ratio ($k_{et}/k_{off} \ll 1$), the scheme reduces to $k_2 = k_{et}K_a$, as discussed above. In the slow-exchange limit, defined by $k_{et}/k_{off} \gg 1$, the rate constant for the second-order ET quenching of unbound, photoexcited ZnMb reduces to the diffusion rate constant ($k_2 \rightarrow k_{on}$).

To apply this model to the experimental results, $K_a = K_0 \exp(-q_{Mb}q_{b_5}f/RT)$, as described in eq 1, and k_{on} is given the charge dependence for diffusion of charged species.[32]

$$k_{on} = k_D^0\{-aq_{Mb}q_{b_5}/[1 - \exp(aq_{Mb}q_{b_5})]\}k_D^0 p(q_{Mb}q_{b_5})$$

(6)

Here k_D^0 is the diffusion-limited rate constant for the proteins that do not interact electrostatically ($-q_{Mb}q_{b_5} = 0$), and p represents the contribution to diffusion from the electrostatic interactions between the partners, with $a = f/RT$.[32] As a simplifying first approximation, we further take k_{et} to be identical for all $[Mb, b_5]$ protein pairs, ignoring the small fractional change observed experimentally (Figure 4, inset). Substitution of eqs 1 and 6 into eq 5 leads to the following form for the dependence of k_2 on the product of the charges, $q_{Mb}q_{b_5}$, where $c = k_D^0/k_{et}$

$$k_2 = k_D^0 p(q_{Mb}q_{b_5}) \times K_a/(cp + K_a)$$

(7)

The fit of eq 7 to the full data set composed of k_2 values measured for the suite of complexes at both pH 7 and 6 (Figure 4, solid line) gives a remarkably good description of its overall dependence on $-q_{Mb}q_{b_5}$, with equivalent scatter in the data at both pH values (Figure 4 and Figure SI_4 of the Supporting Information). This fit is essentially identical to that obtained with the pH 7 data alone (Figure 4, dashed line); the more limited range in $-q_{Mb}q_{b_5}$ available at pH 6 (noted above) makes an independent fit of this data unfeasible.

The following parameters result from the fit of the entire data set to eq 7: $f = RTa = 0.22$ kcal/mol, $c = k_D^0/k_{et} = 17.3$, and $k_D^0 = 2.6 \times 10^8$ M^{-1} s^{-1}. The nominal limiting intracomplex ET rate constant ($k_{et} = k_D^0/c = 1.5 \times 10^7$ s^{-1}) is ~10-fold larger than the intracomplex ET rate constant determined for the SD-type complexes ($k_{et} \sim 10^6$ s^{-1}) (Figure 4 and Table SI_1 of the Supporting Information), suggesting that the rapid intracomplex ET reaction obtained in the quenching measurements (Figure 3) may be dynamically controlled and may actually correspond to a rate constant for conformational interconversion. Motion(s) that might be involved include "diffusion" of b_5 among the ensemble of forms bound to the crp or the conversion between a weakly bound "encounter complex" and the ensemble of bound forms (see the next subsection). The f value of ~0.2 kcal/mol obtained from the fit of k_2 to eq 7 is larger than the f value of ~0.1 kcal/mol determined above from the dependence of K_a on $-q_{Mb}q_{b_5}$. Further work will be required to determine whether this difference merely reflects experimental limitations or whether it reflects the fact that K_a is determined from singlet quenching, while k_2 is determined from triplet quenching, and the two measurements sample different conformational ensembles.

According to eq 5, the SE regime comprises complexes for which $k_{et}/k_{off} \gg 1$ and the FE regime comprises complexes with the reverse of this inequality. Surprisingly, the change between regimes occurs without any apparent transitional behavior at $-q_{Mb}q_{b_5} \sim 16.5$, which corresponds to a k_{et}/k_{off} of ~250, based on the parameters a, k_D^0, and k_{et} determined by the fit to eq 7. To compare this finding with expectations based on the simple model of eq 4, we used the parameters from the fit in Figure 4 to calculate values for k_{on} and k_{off} as a function of $-q_{Mb}q_{b_5}$, and these in turn were used as input parameters for computing kinetic decay traces through numerical solutions of the differential equations for the kinetic scheme of eq 4. The calculated decay traces were then fit to exponential and biexponential decay functions. These fits show that for low values of $-q_{Mb}q_{b_5}$ the simulated traces are monophasic throughout a b_5 titration, whereas for high values of $-q_{Mb}q_{b_5}$ they are biphasic. Of particular note, they further show that the transition from FE to SE kinetic behavior is sharp and occurs at a k_{et}/k_{off} ratio of ~225, very similar to that found experimentally, but at a slightly lower $-q_{Mb}q_{b_5}$ value of ~10.5. This correspondence in the observed and calculated transitions supports the analysis based on the model of eq 4, with the small differences likely attributable to experimental limitations on the ability to detect a second component in the experimental decay traces because of noise on those traces.

BD Simulations. Figure 4 shows that the complex formation and ET reactivity between Mb and b_5 are governed by electrostatic interactions between the total protein charges, viewed as localized in the crp, and that eq 4 provides an excellent global characterization of the response of the kinetic behavior of this system to changes in the protein−protein charge product. To explore the structural basis for this relationship between k_2 and $-q_{Mb}q_{b_5}$, we have performed paired Brownian dynamics (BD) simulations of b_5 docking to the series of Mb mutants created using the three hot spot charge residues. Here, as in previous studies,[12,13] we employ the center-of-mass distance hit criterion (d_{COM}) as a measure of overall binding and a heme propionate−heme propionate distance criterion (d_{OO}) as a measure of reactive binding. The variation of k_2 with $-q_{Mb}q_{b_5}$ can be visualized by comparing the number of reactive OO hits to the number of COM hits (R), with an expectation that the two numbers approach unity as the energy landscape approaches the SD limit in which all hits are reactive.

Figure SI_2 of the Supporting Information shows the numbers of hits from the two types of simulations as a function of $-q_{Mb}q_{b_5}$. With the COM criterion, nearly half of the 10^4 trajectories result in hits, even for the $[Mb(wt), b_5]$ complex where $-q_{Mb}q_{b_5} \sim 0$, and this number increases only modestly as a function of increasing $-q_{Mb}q_{b_5}$. However, the number of hits with the OO criterion is quite low when $-q_{Mb}q_{b_5}$ is small, increases rapidly as $-q_{Mb}q_{b_5}$ increases, and approaches the COM value as a limiting value at high $-q_{Mb}q_{b_5}$ values.

The global response of k_2 to changes in $-q_{Mb}q_{b_5}$ is accompanied by noticeable variations (granularity) at fixed values of $-q_{Mb}q_{b_5}$, which offers additional insights into the overall progression. For example, Figure 4 contains 12 reaction pairs with a $-q_{Mb}q_{b_5}$ of 19.5 ± 2, among which k_2 varies by roughly 1 order of magnitude, and similar behavior is observed for the five pairs with a $-q_{Mb}q_{b_5}$ of 7.5 ± 2. BD simulations indicate that the variation in k_2 at a given value of $-q_{Mb}q_{b_5}$ is not reflective of experimental uncertainties but arises because the interactions within each pair involve an ensemble of conformations with b_5 bound within the crp, and the nature of the ensemble depends on the number and placement of the surface charges.

The variations in the nature of these ensembles can be understood by comparing "hit profiles" from Brownian dynamics simulations for protein pairs with similar $-q_{Mb}q_{b_5}$

values. The insets in Figure 6 show profiles of the reactive hits for the FE/DD-type $[Mb(wt), b_5]$ complex and three SE/SD-
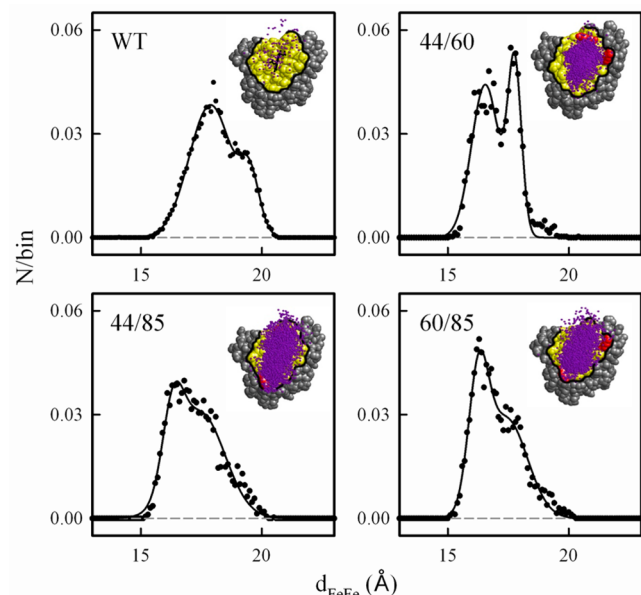

Figure 6. BD hit profiles (insets) and corresponding d_{FeFe} histograms for Mb(wt) and Mb(+4) mutants with a $-q_{Mb}q_{b_5}$ of 19.5. The number of counts per bin was normalized to the total number of hits, and the resulting histograms were fit to a sum of two Gaussians (Table 1). Conditions: OO reaction criterion with a 4.0 Å distance cutoff, pH 7, μ = 18 mM, 20 °C, 10^4 trajectories, 0.1 Å distance binning. To improve the signal:noise ratio on the histogram for the Mb(wt) complex, a simulation with 10^6 trajectories was used.

type $[Mb(+4), b_5]$ complexes with a $-q_{Mb}q_{b_5}$ of ~19.5 that involve different pairs of altered hot spot residues. For each of these $[Mb(+4), b_5]$ complexes, the reactive hits have coalesced from the dispersed array seen for the complex with Mb(wt)[13] into a "reactive" ensemble ("cluster") of hits in the crp, with the majority of the hits having the requisite short metal–metal distance needed for rapid ET. However, the histograms of the metal–metal distances for the hit ensembles of these three complexes are significantly different.

Viewed qualitatively, the distributions for the complexes with Mb(44/85) and Mb(60/85) are expanded in comparison to the distribution for the complex with Mb(44/60), extending toward the E85 hot spot mutation site. Examined more quantitatively, the histograms for each of the three Mb(+4) mutants are described well by a sum of two Gaussian functions with peak maxima near 16.5 and 17.5 Å (Table 1). While the

Table 1. Parameters from Double Gaussian Fits to d_{FeFe} Histograms from BD Simulations[a]

	peak 1			peak 2		
protein	d_{max} (Å)	$\Delta w_{1/2}$ (Å)	h^b	d_{max} (Å)	$\Delta w_{1/2}$ (Å)	h^b
Mb(wt)	17.9	0.88	0.038	19.5	0.40	0.015
Mb(44/60)	16.5	0.57	0.044	17.8	0.28	0.049
Mb(44/85)	16.3	0.43	0.023	17.5	1.0	0.030
Mb(60/85)	16.3	0.41	0.036	17.4	0.86	0.029

[a]OO reaction criterion, d_{OO} = 4.0; 0.1 Å bins. [b]Amplitudes based on 10^6 trajectories (wt) or 10^4 trajectories (mutants).

breadths of the distributions for the shorter distance component (peak 1) are quite similar among the three pairs, the width at half-maximum ($\Delta w_{1/2}$) for the longer-range component (peak 2) is much smaller for the $[Mb(44/60), b_5]$ pair than it is for the other two pairs. Thus, the differences in the hit profiles largely arise from differences in the less reactive, longer-range component and in the relative populations of the short- and long-range components. Overall, these computations confirm that increasing the charge of the crp serves to increase the degree of attraction of the b_5 partner to this Mb surface region, but variation in the location of the charges within the crp introduces granularity into the details of the ensemble of contributing conformations.

It is useful to note that this granularity exists within the context of a design strategy that successfully enhances binding and reactivity by making variants with an increased total charge. By localizing all mutation sites within the crp, this design strategy generates a progression in charge product while minimizing granularity. With alternative design strategies, it is conceivable that the granularity in k_2 at a fixed $-q_{Mb}q_{b_5}$ could be made to encompass the full range of behaviors seen in the progression, thus illuminating the importance of the overall pattern of charged residues. Indeed, such an alternative strategy was elegantly implemented by Margoliash and co-workers,[55−58] who mapped the binding interface of Cc with several of its redox partners through kinetic measurements of ET that employed a suite of site-selective, chemically modified Cc proteins in which the dipole moment of Cc was varied while the charge was fixed.

Generality of the Pre-Equilibrium Model of eq 4. It is widely thought that the association and docking of protein partners is a complicated process, with the partners first forming an encounter complex before proceeding to the most stable bound state.[23,47,59−62] Nonetheless, application of the analysis based on the pre-equilibrium binding/ET scheme of eq 4 to the $[RC, c_2]$ complex suggests that this simple approach offers a general basis for discussions of protein–protein ET within suites of mutants formed by varying the properties of one or both of the partners. For the $[Mb, b_5]$ system, the linear relationship between charge product $-q_{Mb}q_{b_5}$ and the driving force for binding $[-\Delta G_a = RT \log K_a$ (eq 1)] allows the abscissa of the semilogarithmic plot of k_2 to be assigned to either $-\Delta G_a$ or $-q_{Mb}q_{b_5}$ (Figure 4, top and bottom axes). The use of a free energy axis then permits a comparison of the behavior of the $[Mb, b_5]$ system with ET between other suites of partners where the driving force for binding is varied without such a simple correlation with total charge product.

The pre-eminent example of such a study involved measurements by Okamura and co-workers of ET between c_2 and a suite of variants of the RC. Guided by the crystallographic structure of the $[RC, c_2]$ complex,[63] they initially prepared charged RC interface mutants (Δq = −1, 1, 2, and 4) to study long-range electrostatic effects on the formation, stabilization, and reactivity of the $[RC, c_2]$ complex.[18,19] As the crystal structure of the $[RC, c_2]$ complex suggested the presence of hydrophobic residues in the core of the binding interface, they subsequently prepared RC single-site variants at three hydrophobic hot spot positions.[20]

The inset of Figure 7 presents values of k_2 for ET between c_2 and the suite of RC variants prepared by mutating hydrophobic residues without changing the charge. The parent $[RC, c_2]$ complex is so tightly bound that despite the large decreases in
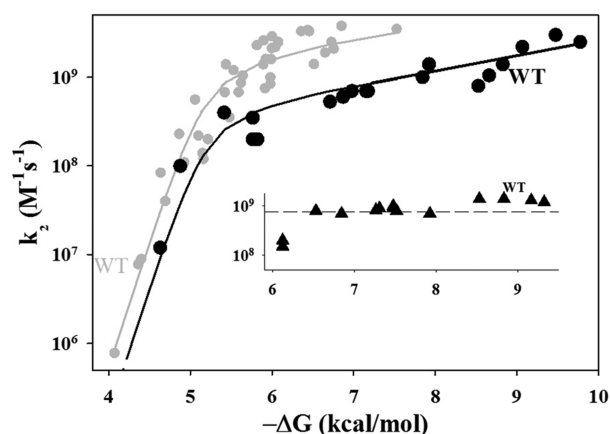
Figure 7. Progression in k_2 as a function of K_a for $[Mb, b_5]$ (gray) and $[RC, c_2]$ (black) complexes. Data for charged RC mutants are from ref 19; data for hydrophobic mutants (inset) are from ref 20. The data point for the LK(M191) mutant is included with the charged mutants rather than the hydrophobics. The curve through the data for the $[RC, c_2]$ complex is drawn to guide the eye.

binding affinity that were achieved, all the complexes from this suite remain in the SE regime. For this regime, the pre-equilibrium model predicts that $k_2 = k_{on} \sim k_D$. As k_D should be independent of the binding free energy for complexes in which the RC differs only through hydrophobic mutations, k_2 should be invariant in this regime, exactly as observed. In short, within this suite, the reactivity is kinetically decoupled from the large changes in binding.

The study with the charge-altering RC variation corresponds more closely to this work with the $[Mb, b_5]$ complex. Figure 7 shows the variation of k_2 as a function of $RT \ln K_a = -\Delta G_a$ for the suite of RC with charge-altering mutations. As the binding is weakened by mutation, the tightly bound complex shifts from the SE regime into the FE regime in a progression that reverses the progression from FE to SE generated by the charge-reversal mutations in the weakly bound $[Mb, b_5]$ complex. An independent fit of k_2 versus $-\Delta G_a$ for the $[RC, c_2]$ complex to eq 7 is not feasible, as there are too few points in the FE regime, but the variation of k_2 for the $[RC, c_2]$ complexes with $-\Delta G_a$, nonetheless, is described well by offsetting the fitting curve for the $[Mb, b_5]$ pair. The offset to lower k_2 reflects, in part, a smaller value of k_{et}, as might be expected because the bacteriochlorophyll special pair of the RC is buried whereas the Mb heme edge is exposed.

Unlike the driving force for the $[Mb, b_5]$ system, $-\Delta G_a$ for the $[RC, c_2]$ complexes does not monotonically follow the nominal mutation-induced changes in RC charge. This difference likely occurs because the "binding patch" of the RC (Figure SI_3 of the Supporting Information) is quite large in comparison with the crp of Mb, and the charged residues on the RC reactive surface are dispersed within this much larger area. In addition, the crp of c_2 is small compared to the RC binding surface, in contrast to the excellent match between the crp of Mb and b_5. As a result, the binding interfaces between c_2 and different modified RCs will involve residues in different electrostatic microenvironments, with different solvent exposure and different degrees of screening. As a consequence, charge-changing mutations at different sites will have different influences on binding, preventing any simple correlation between the binding driving force and the product of total charges. Furthermore, the binding affinities for the RC

hydrophobic variants span an equally large range in $-\Delta G_a$ as do the complexes with the RC charge variants, yet the hydrophobic variations do not "push" the complex appreciably into the FE regime, whereas the charge variations do.

The large variability in the influence of individual contacts within the $[RC, c_2]$ interface contrasts with the considerably smaller variability and/or granularity for $[Mb, b_5]$ complexes, discussed above. This difference reflects the fact that the BD-designed Mb mutation sites are not dispersed over a large binding surface, as with the RC, but by design are closely clustered within the small Mb crp.

■ SUMMARY AND CONCLUSIONS

We have examined photoinitiated ET quenching within a set of $[ZnMb, b_5]$ complexes prepared from Mb variants identified by our interface electrostatic redesign strategy. The addition of positive charges to the reactive region of the Mb surface through D/E → K charge-reversal mutations at one, two, or all three of the hot spot positions (D44, D60, and E85), augmented with variants in which negative charge is eliminated from the Mb or b_5 surface by neutralization of their heme propionates, has produced a remarkably large range in the product of the total charges of the two partners ($-5 < -q_{Mb}q_{b_5} < 40$). As $-q_{Mb}q_{b_5}$ is increased within this range, the affinity constant for binding of b_5 to Mb increases by 10^3 and the complex undergoes a transition from FE to SE kinetic behavior on the triplet ET time scale. The second-order triplet ET quenching rate constant (k_2) is measurable throughout the entire $-q_{Mb}q_{b_5}$ range, increasing progressively as $-q_{Mb}q_{b_5}$ increases. The rate constant for intracomplex protein−protein ET from the ^3ZnP excited state of the ZnMb (k_{et}) can be directly measured only for complexes in the SE regime where it increases by roughly 1 order of magnitude (Figure 4, inset). Furthermore, intracomplex ET from the singlet excited state used here to measure the binding constants for the complex (K_a) becomes progressively more effective with increasing total charge product. Indeed, the singlet ET process has been directly monitored on the nanosecond to picosecond time scale for the $[Mb, b_5]$ complex with the highest $-q_{Mb}q_{b_5}$ value.[11]

The binding affinity (K_a), which probes the population of ET-active configurations of the $[Mb, b_5]$ complex, shows a simple, exponential dependence on $-q_{Mb}q_{b_5}$ (Figure 4 and eq 1). To understand this behavior, we introduced the idea of a charged reactive patch (crp) on the surface of each partner: the compact surface area around the heme edge that contains a charge equal to the total charge of the wild-type protein and encompassing much of the reactive surface region (Rr). All of the Mb mutation sites employed in this study fall within the crp (Figure 5A), so the total charge on every Mb charge variant can be treated as being concentrated within this surface region. A corresponding crp for b_5 and its heme-neutralized charge variant likewise contains the total b_5 charge and its good ET pathways (Figure SI_1 of the Supporting Information). The definition of crp naturally leads to a picture in which the ET partners react only when the Rr within the two complementary crp's are electrostatically drawn together.

The progression in k_2 with an increasing $-q_{Mb}q_{b_5}$ and the transition from FE to SE kinetic behavior (Figure 4) can be understood by integrating the crp description of a protein−protein interface and the corresponding charge product dependencies of the binding free energy (eq 1) and association

rate (eq 6) into the simplest steady-state, pre-equilibrium treatment of reversible binding between the ET partners (eq 4). The suite of complexes studied here is found to encompass the full range of behaviors predicted by the model, and as shown in Figure 4, its simple approach captures the global aspects of the correlated electrostatic control of binding and reactivity extremely well. At the same time, it reveals a granularity in the dependence of k_2 on total charge product, the variations in k_2 at a fixed $-q_{Mb}q_{b_s}$. As illustrated in Figure 6, this variation results from a response of the populations of different bound configurations to variations in the electrostatic surface potentials resulting from the alternative arrangements of charges within the Mb crp.

The general applicability of this simple, textbook, pre-equilibrium model to suites of ET complexes prepared with surface mutants is supported by its ability to fully describe the behavior of ET for suites of [RC, c_2] complexes. The analysis reveals a strong difference between the behavior of the hydrophobic RC mutants and the electrostatic RC mutants, yet the behavior of both subsets can be explained with the pre-equilibrium model. The model further illuminates the basis of the strong variation in the response of the binding affinity to mutations at different sites on the RC surface.

In summary, guided by the BD−mutation surface redesign strategy, we have made considerable progress in electrostatically strengthening the binding of the intrinsically, weakly bound [Mb, b_5] complex, thereby coupling reactivity to binding at the crp as the total charge product, $-q_{Mb}q_{b_s}$, is increased. The example set by the tightly bound [RC, c_2] complex shows how much more remains to be achieved in strengthening the binding of the [Mb, b_5] complex, further pushing it toward the SD limit where NMR structure determination or even crystallization of a tightly bound complex will offer a welcome comparison to the ensemble of structures predicted by the BD simulations. It is further anticipated that the strengthened binding will be accompanied by the direct observation of enhanced ultrafast ET on the singlet time scale. As a complement to these efforts, we are employing computational approaches to understand the dynamic and structural factors that govern protein−protein recognition and ET. In particular, the integration of interprotein pathways and molecular dynamics with Brownian dynamics ensemble generation[51] provides a promising approach for further exploring the heterogeneity in the electrostatic interactions within the protein−protein interface that govern the progression in behaviors of the [Mb, b_5] complex, and others, and the additional granularity that is not incorporated in the model presented here.

■ ASSOCIATED CONTENT

⑤ Supporting Information

Four figures that present additional experimental data and pictures of the charged reactive patches and one table of kinetic parameters. This material is available free of charge via the Internet at http://pubs.acs.org.

■ AUTHOR INFORMATION

Corresponding Author

*E-mail: bmh@northwestern.edu. Phone: (847) 491-3104. Fax: (847) 491-7713.

■ ABBREVIATIONS

Mb, myoglobin; b_5, cytochrome b_5; RC, photosynthetic reaction center; c_2, cytochrome c_2; DD, dynamic docking; SD, simple docking; FE, fast exchange; SE, slow exchange; ET, electron transfer; crp, charged reactive patch; Rr, reactive region; BD, Brownian dynamics.

■ REFERENCES

(1) Janin, J. (1997) The kinetics of protein-protein recognition. *Proteins: Struct., Funct., Genet. 28*, 153−161.

(2) Keskin, O., Gursoy, A., Ma, B., and Nussinov, R. (2008) Principles of protein-protein interactions: What are the preferred ways for proteins to interact? *Chem. Rev. 108*, 1225−1244.

(3) Ryan, D. P., and Matthews, J. M. (2005) Protein-protein interactions in human disease. *Curr. Opin. Struct. Biol. 15*, 441−446.

(4) Percy, M. J., and Lappin, T. R. (2008) Recessive congenital methaemoglobinaemia: Cytochrome b_5 reductase deficiency. *Br. J. Haematol. 141*, 298−308.

(5) Zacharias, M., Ed. (2010) *Protein-Protein Complexes: Analysis, Modeling and Drug Design*, Imperial College Press, London.

(6) Nussinov, R., and Schreiber, G. (2009) *Computational protein-protein interactions*, CRC Press, Boca Raton, FL.

(7) Liang, Z.-X., Kurnikov, I. V., Nocek, J. M., Mauk, A. G., Beratan, D. N., and Hoffman, B. M. (2004) Dynamic Docking and Electron-Transfer between Cytochrome b_5 and a Suite of Myoglobin Surface-Charge Mutants. Introduction of a Functional-Docking Algorithm for Protein-Protein Complexes. *J. Am. Chem. Soc. 126*, 2785−2798.

(8) Naito, A., Hui, H. L., Noble, R. W., and Hoffman, B. M. (2001) Determination of the Hemoglobin Surface Domains that React with Cytochrome b_5. *Biochemistry 40*, 2060−2065.

(9) Wheeler, K. E., Nocek, J., Cull, D. A, Yatsunyk, L. A., Rosenzweig, A. C., and Hoffman, B. M. (2007) Dynamic Docking of Cytochrome b$_5$ with Myoglobin and α-Hemoglobin: Heme-Neutralization 'Squares' and the Binding of Electron-Transfer-Reactive Configurations. *J. Am. Chem. Soc. 129*, 3906−3917.

(10) Nocek, J. M., and Hoffman, B. M. (2010) Dynamic Docking (DD). In *Encyclopedia of Biophysics* (Roberts, G. C., Ed.) Springer, New York.

(11) Xiong, P., Nocek, J. M., Vura-Weis, J., Lockard, J. V., Wasielewski, M. R., and Hoffman, B. M. (2010) Faster Interprotein Electron Transfer in a [Myoglobin, b_5] Complex with a Redesigned Interface. *Science 330*, 1075−1078.

(12) Xiong, P., Nocek, J. M., Griffin, A. K. K., Wang, J., and Hoffman, B. M. (2009) Electrostatic Redesign of the [Myoglobin, Cytochrome b$_5$] Interface To Create a Well-Defined Docked Complex with Rapid Interprotein Electron Transfer. *J. Am. Chem. Soc. 131*, 6938−6939.

(13) Nocek, J. M., Knutson, A. K., Xiong, P., Co, N. P., and Hoffman, B. M. (2010) Photoinitiated Singlet and Triplet Electron Transfer Across a Re-Designed [Myoglobin, Cytochrome b$_5$] Interface. *J. Am. Chem. Soc. 132*, 6165−6175.

(14) Kortemme, T., and Baker, D. (2002) A simple physical model for binding energy hot spots in protein-protein complexes. *Proc. Natl. Acad. Sci. U.S.A. 99*, 14116−14121.

(15) Kortemme, T., Kim, D. E., and Baker, D. (2004) Computational alanine scanning of protein-protein interfaces. *Sci. STKE 2004*, l2.

(16) Schreiber, G., and Fersht, A. R. (1995) Energetics of protein-protein interactions: Analysis of the barnase-barstar interface by single mutations and double mutant cycles. *J. Mol. Biol. 248*, 478−486.

(17) Shaul, Y., and Schreiber, G. (2005) Exploring the charge space of protein-protein association: A proteomic study. *Proteins: Struct., Funct., Bioinf. 60*, 341−352.

(18) Tetreault, M., Cusanovich, M., Meyer, T., Axelrod, H., and Okamura, M. Y. (2002) Double Mutant Studies Identify Electrostatic Interactions That Are Important for Docking Cytochrome c_2 onto the Bacterial Reaction Center. *Biochemistry 41*, 5807−5815.

(19) Tetreault, M., Rongey, S. H., Feher, G., and Okamura, M. Y. (2001) Interaction between Cytochrome c_2 and the Photosynthetic Reaction Center from *Rhodobacter sphaeroides*: Effects of Charge-Modifying Mutations on Binding and Electron Transfer. *Biochemistry 40*, 8452−8462.

(20) Gong, X.-M., Paddock, M. L., and Okamura, M. Y. (2003) Interactions between cytochrome c_2 and photosynthetic reaction center from *Rhodobacter sphaeroides*: Changes in binding affinity and electron transfer rate due to mutation of interfacial hydrophobic residues are strongly correlated. *Biochemistry 42*, 14492−14500.

(21) Liang, Z.-X., Jiang, M., Ning, Q., and Hoffman, B. M. (2002) Dynamic Docking and Electron Transfer Between Myoglobin and Cytochrome b_5. *JBIC, J. Biol. Inorg. Chem. 7*, 580−588.

(22) Nocek, J. M., Sishta, B. P., Cameron, J. C., Mauk, A. G., and Hoffman, B. M. (1997) Cyclic Electron Transfer within the [Zn-deuteromyoglobin, Cytochrome b_5] Complex: Redox-Linked Changes at the Interface. *J. Am. Chem. Soc. 119*, 2146−2155.

(23) Ubbink, M. (2012) Dynamics in transient complexes of redox proteins. *Biochem. Soc. Trans. 40*, 415−418.

(24) Worrall, J. A. R., Liu, Y., Crowley, P. B., Nocek, J., Hoffman, B. M., and Ubbink, M. (2002) Myoglobin and Cytochrome b_5: A Nuclear Magnetic Resonance Study of a Highly Dynamic Protein Complex. *Biochemistry 41*, 11721−11730.

(25) Warshel, A., and Russell, S. T. (1984) Calculations of electrostatic interactions in biological systems and in solutions. *Q. Rev. Biophys. 17*, 283−422.

(26) Sharp, K. A., and Honig, B. (1990) Electrostatic Interactions in Macromolecules: Theory and Applications. *Annu. Rev. Biophys. Biophys. Chem. 19*, 301−332.

(27) Honig, B., and Nicholls, A. (1995) Classical Electrostatics in Biology and Chemistry. *Science 268*, 1144−1149.

(28) Northrup, S. H., Allison, S. A., and McCammon, J. A. (1984) Brownian dynamics simulation of diffusion-influenced bimolecular reactions. *J. Chem. Phys. 80*, 1517−1524.

(29) Tiede, D. M., Vashishta, A., and Gunner, M. R. (1993) Electron-Transfer Kinetics and Electrostatic Properties of the *Rhodobacter sphaeroides* Reaction Center and Soluble c-Cytochromes. *Biochemistry 32*, 4515−4531.

(30) Ullmann, G. M., and Kostic, N. M. (1995) Electron-Tunneling Paths in Various Electrostatic Complexes between Cytochrome c and Plastocyanin. Anisotropy of the Copper-Ligand Interactions and Dependence of the Iron-Copper Electronic Coupling on the Metalloprotein Orientation. *J. Am. Chem. Soc. 117*, 4766−4774.

(31) Schneidman-Duhovny, D., Inbar, Y., Nussinov, R., and Wolfson, H. J. (2005) PatchDock and SymmDock: Servers for rigid and symmetric docking. *Nucleic Acids Res. 33*, W363−W367.

(32) Steinfeld, J. I., Francisco, J. S., and Hase, W. L. (1999) *Chemical Kinetics and Dynamics*, 2nd ed., Prentice-Hall, Inc., Upper Saddle River, NJ.

(33) Espenson, J. H. (1981) *Chemical Kinetics and Reaction Mechanisms*, McGraw-Hill, New York.

(34) Atkins, P. W. (1986) *Physical Chemistry*, 3rd ed., W. H. Freeman and Co., New York.

(35) Guillemette, J. G., Matsushima-Hibiya, Y., Atkinson, T., and Smith, M. (1991) Expression in *Escherichia coli* of a synthetic gene coding for horse heart myoglobin. *Protein Eng. 4*, 585−592.

(36) Ribeiro, E. A., Jr., Regis, W. C. B., Tasic, L., and Ramos, C. H. I. (2003) Fast purification of the apo form and of a non-binding heme mutant of recombinant sperm whale myoglobin. *Protein Expression Purif. 28*, 202−208.

(37) Antonini, E., and Brunori, M. (1971) *Hemoglobin and Myoglobin in Their Reactions with Ligands*, North Holland Publishing Co., Amsterdam.

(38) Lloyd, E., Ferrer, J. C., Funk, W. D., Mauk, M. R., and Mauk, A. G. (1994) Recombinant Human Erythrocyte Cytochrome b_5. *Biochemistry 33*, 11432−11437.

(39) Funk, W. D., Lo, T. P., Mauk, M. R., Brayer, G. D., MacGillivray, R. T. A., and Mauk, A. G. (1990) Mutagenic, electrochemical, and crystallographic investigation of the cytochrome b_5 oxidation-reduction equilibrium: Involvement of asparagine-57, serine-64, and heme propionate-7. *Biochemistry 29*, 5500−5508.

(40) Tanford, C., and Kirkwood, J. G. (1957) Theory of protein titration curves. I. General equations for impenetrable spheres. *J. Am. Chem. Soc. 79*, 5333−5339.

(41) Northrup, S. H., Thomasson, K. A., Miller, C. M., Barker, P. D., Eltis, L. D., Guillemette, J. G., Inglis, S. C., and Mauk, A. G. (1993) Effects of Charged Amino Acid Mutations on the Bimolecular Kinetics of Reduction of Yeast Iso-1-ferricytochrome c by Bovine Ferrocytochrome b_5. *Biochemistry 32*, 6613−6623.

(42) Kao, Y. H., Fitch, C. A., Bhattacharya, S., Sarkisian, C. J., Lecomte, J. T. J., and Garcia-Moreno, B. (2000) Salt effects on ionization equilibria of histidines in myoglobin. *Biophys. J. 79*, 1637−1654.

(43) Bhattacharya, S., and Lecomte, J. T. J. (1997) Temperature dependence of histidine ionization constants in myoglobin. *Biophys. J. 73*, 3241−3256.

(44) Ozols, J., and Strittmatter, P. (1964) The Interaction of Porphyrins and Metalloporphyrins with Apocytochrome b_5. *J. Biol. Chem. 239*, 1018−1023.

(45) Hoffman, B. M., Celis, L. M., Cull, D. A., Patel, A. D., Seifert, J. L., Wheeler, K. E., Wang, J., Yao, J., Kurnikov, I. V., and Nocek, J. (2005) Differential Influence of Dynamic Processes on Forward and Reverse Electron Transfer Across a Protein-Protein Interface. *Proc. Natl. Acad. Sci. U.S.A. 102*, 3564−3569.

(46) Berg, O. G., and von Hippel, P. H. (1985) Diffusion-Controlled Macromolecular Interactions. *Annu. Rev. Biophys. Biophys. Chem. 14*, 131−160.

(47) Schreiber, G., Haran, G., and Zhou, H.-X. (2009) Fundamental Aspects of Protein-Protein Association Kinetics. *Chem. Rev. 109*, 839−860.

(48) See discussions of Van Leeuwen (49) and by Zhou et al. (50).

(49) Van Leeuwen, J. W. (1983) The ionic strength dependence of the rate of a reaction between two large proteins with a dipole moment. *Biochim. Biophys. Acta 743*, 408−421.

(50) Zhou, J. S., and Kostic, N. M. (1992) Photoinduced Electron-Transfer Reaction in a Ternary System Involving Zinc Cytochrome c and Plastocyanin. Interplay of Monopolar and Dipolar Electrostatic Interactions between Metalloproteins. *Biochemistry 31*, 7543−7550.

(51) Keinan, S., Nocek, J. M., Hoffman, B. M., and Beratan, D. N. (2012) Interfacial Hydration, Dynamics and Electron Transfer: Multi-Scale ET Modeling of the Transient [Myoglobin, Cytochrome b_5] Complex. *Phys. Chem. Chem. Phys. 14*, 13881−13889.

(52) Liang, Z.-X., Nocek, J., Huang, K., Hayes, R. T., Kurnikov, I. V., Beratan, D. N., and Hoffman, B. M. (2002) Dynamic Docking and Electron Transfer Between Zn-myoglobin and Cytochrome b_5. *J. Am. Chem. Soc. 124*, 6849−6859.

(53) Warshel, A., and Dryga, A. (2011) Simulating electrostatic energies in proteins: Perspectives and some recent studies of pK$_a$s, redox, and other crucial functional properties. *Proteins: Struct., Funct., Bioinf. 79*, 3469−3484.

(54) Gunner, M. R., Mao, J., Song, Y., and Kim, J. (2006) Factors influencing the energetics of electron and proton transfers in proteins. What can be learned from calculations? *Biochim. Biophys. Acta 1757*, 942−968.

(55) Speck, S. H., Koppenol, W. H., Dethmers, J. K., Osheroff, N., Margoliash, E., and Rajagopalan, K. V. (1981) Definition of cytochrome c binding domains by chemical modification. Interaction of horse cytochrome c with beef sulfite oxidase and analysis of steady state kinetics. *J. Biol. Chem. 256*, 7394−7400.

(56) Koppenol, W. H., and Margoliash, E. (1982) The Asymmetric Distribution of Charges on the Surface of Horse Cytochrome c. Functional Implications. *J. Biol. Chem. 257*, 4426−4437.

(57) Speck, S. H., Ferguson-Miller, S., Osheroff, N., and Margoliash, E. (1979) Definition of cytochrome c binding domains by chemical modification. 5. Kinetics of reaction with beef mitochondrial reductase and functional organization of the respiratory chain. *Proc. Natl. Acad. Sci. U.S.A. 76*, 155−159.

(58) Margoliash, E., and Bosshard, H. R. (1983) Guided by electrostatics, a textbook protein comes of age. *Trends Biochem. Sci. 8*, 316−320.

(59) Schreiber, G. (2002) Kinetic studies of protein-protein interactions. *Curr. Opin. Struct. Biol. 12*, 41−47.

(60) Spaar, A., Dammer, C., Gabdoulline, R. R., Wade, R. C., and Helms, V. (2006) Diffusional encounter of barnase and barstar. *Biophys. J. 90*, 1913−1924.

(61) Miyashita, O., Onuchic, J. N., and Okamura, M. Y. (2004) Transition state and encounter complex for fast association of cytochrome c_2 with bacterial reaction center. *Proc. Natl. Acad. Sci. U.S.A. 101*, 16174−16179.

(62) Alsallaq, R., and Zhou, H.-X. (2008) Electrostatic rate enhancement and transient complex of protein-protein association. *Proteins: Struct., Funct., Bioinf. 71*, 320−335.

(63) Axelrod, H. L., Abresch, E. C., Okamura, M. Y., Yeh, A. P., Rees, D. C., and Feher, G. (2002) X-ray Structure Determination of the Cytochrome c_2: Reaction Center Electron Transfer Complex from *Rhodobacter sphaeroides*. *J. Mol. Biol. 319*, 501−515.